ISBN: 978-3-95450-227-1 ISSN: 2673-5490 doi:10.18429/JACoW-IPAC2022-THPOMS028

PERFORMANCE STUDY OF THE NIMMS SUPERCONDUCTING COMPACT SYNCHROTRON FOR ION THERAPY WITH STRONGLY CURVED MAGNETS

H. X.Q. Norman*[1,2], R. B. Appleby[1], University of Manchester, Manchester, UK
S. L. Sheehy[3], University of Melbourne, Melbourne, Australia
E. Benedetto, SEEIIST Association, Geneva, Switzerland
M. Karppinen, CERN, Geneva, Switzerland
H. L. Owen[1], STFC Daresbury Laboratory, Warrington, UK
[1]also at Cockcroft Institute, Warrington, UK
[2]also at University of Melbourne, Melbourne, Australia
[3]also at Australian Nuclear Science and Technology Organisation (ANSTO), Australia

Abstract

Delivery of heavy ion therapy currently utilises normal conducting synchrotrons. For the future generation of clinical facilities, the accelerator footprint must be reduced while adopting beam intensities above 1×10^{10} particles per spill for more efficient, effective treatment. The Next Ion Medical Machine Study (NIMMS) is investigating the feasibility of a compact (27 m circumference) superconducting synchrotron, based on 90° alternating-gradient, canted-cosine-theta magnets to meet these criteria. The understanding of the impact of the higher order multipole fields of these magnets on the beam dynamics of the ring is crucial for optimisation of the design and to assess its performance for treatment. We analyse the electromagnetic model of a curved superconducting magnet to extract its non-linear components. Preliminary assessment is performed using MADX/PTC. Further scope, involving cross-referencing with other particle tracking codes, is discussed.

INTRODUCTION

The Next Ion Medical Machine Study (NIMMS) is a CERN-based initiative for the development of accelerators and supporting technology for future hadron therapy facilities. A compact synchrotron design, based on 90° superconducting (SC) alternating-gradient, canted-cosine-theta (AG-CCT) magnets has been proposed [1]. Due to the coil geometry of the magnets, one can achieve high quality, combined-function dipole and quadrupole fields by nesting quadrupole layers within each dipole magnet [2]. This reduces the circumference of the accelerator to ≈ 27 m, as shown in Fig. 1.

The design motivation is for delivery of carbon ion therapy (energies ranging from 100 MeV/u to 430 MeV/u), which is not widely available despite clinical benefits compared with proton therapy and x-ray radiotherapy [3]. By employing AG-CCT magnets in the four bending sections (operating at $B_{\mathrm{dip}} = 3.5$ T), the size and weight of the accelerator is reduced, as well as building and operation costs. The configuration achieves strong focusing, reducing maximum dispersion to 2.5 metres. To realise the design for future facilities, a detailed magnet model is needed, subject to clinical and technical requirements of the accelerator. An electromagnetic (EM) AG-CCT model is anticipated.

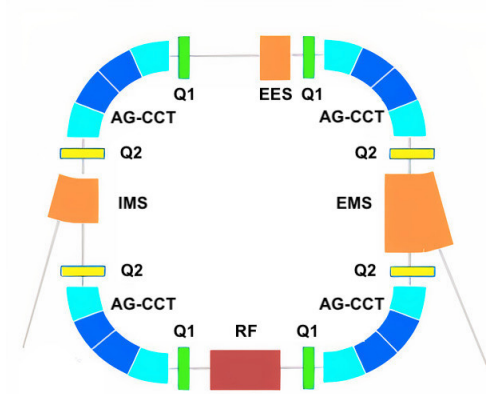

Figure 1: 27 m circumference superconducting synchrotron. The elements are: AG-CCT magnets (blue, outer corners of the ring, dark blue quadrupole layers centered); injection and extraction septa (IMS, EES, EMS) (orange, left-middle, right-middle and top-centre); RF cavity (red, bottom-centre); tuning quadrupoles (yellow and green, either side of the AG-CCT magnets, septa and RF). Modified from [1].

In this study, we develop the numerical analysis tools needed to extract multipole fields from the prospective AG-CCT magnet to understand their impact on the performance of the NIMMS synchrotron. We first analyse a complementary cosine-theta (CT) magnet model; numerical methods are used to extract multipole fields from simulated magnetic field maps, which are then incorporated into the accelerator lattice for beam dynamics simulations using MAD-X [4]. The analysis tools developed during this study will be applied to a future AG-CCT EM model to assess the effect of its multipole fields on the beam dynamics of the ring, and if it is clinically suitable.

* hannah.norman@manchester.ac.uk

ISBN: 978-3-95450-227-1 ISSN: 2673-5490 doi:10.18429/JACoW-IPAC2022-THPOMS028

MAGNET DETAILS

CT Option

A 30°, combined-function (CF) CT demonstrator has been proposed by NIMMS for a compact SC gantry [5]. The magnet operates at a dipole field = 3 T with a quadrupole gradient = 3.5 T/m generated by slight asymmetry in the geometry [6]. Compared with CCT magnets, the coils are wound in a singular layer, instead of two oppositely canted layers wound around a supporting structure [7].

Magnetic Field Theory

Higher order field errors (harmonics) are present due to physical imperfections and saturation. The magnetic field is decomposed to examine the distribution of these harmonics. A 2D representation of the field over (x, y) accurately describes the field over the magnet body; a multipole expansion of **B** in polar coordinates was conducted. The "normal" and "skew" multipole coefficients (B_n, A_n) are returned via fast Fourier transform (FFT) [8].

$$B_r(r,\theta) = \sum_{n=1}^{\infty} \left(\frac{r}{R_{\text{ref}}}\right)^{(n-1)} [B_n \sin n\theta + A_n \cos n\theta] \quad (1)$$

$$B_\theta(r,\theta) = \sum_{n=1}^{\infty} \left(\frac{r}{R_{\text{ref}}}\right)^{(n-1)} [B_n \sin n\theta - A_n \cos n\theta] \quad (2)$$

In straight coordinate systems, the multipole coefficients are equivalent to taking derivatives of the field on axis; these differ in the curved case. It has been recently described that multipole expansion is not mathematically valid for curved magnets [9]; instead we use derivatives, which allow us to directly relate the multipoles to the field composition. The relationship is given by

$$B_{n+1}(r,\theta) = \frac{R_{\text{ref}}^n}{n!} \left(\frac{\partial^n B_y}{\partial x^n}\right)\Big|_{x=0,y=0} \Bigg\} n \geq 0 \quad (3)$$

Electromagnetic Study

We examine a model of the magnet in OPERA-3D [10]; a 3D field map over the body of the magnet is taken to calculate the multipoles. A polynomial curve is fitted to the main field in the magnet body (B_y) in Python as an initial calculation; the coefficients give the derivatives which are compared with previously calculated multipoles in [6], via Eqs. (1,2). The results from the two methods were first compared for a straight version of the CT magnet, which had good agreement. The results from both methods for the straight and curved magnets are presented in Table 1 at a reference radius R_{ref} = 20 mm, 2/3 of the bore radius. The integrated harmonics are on the order of 10^{-4} with an expected large b_2 due to the quadrupole field gradient. It is worth noting that the fit accuracy breaks down; the presence of higher order multipoles affects the values of the multipoles that are included in the fit [11], hence the discrepancies in b_2 and b_4 for the straight case. For our highest order of interest (b_4 = octupole), the polynomial fit multipoles for the curved CT magnet are added to the bending magnets in MAD-X.

Table 1: Integrated Harmonics for Straight and Curved (focusing) CT Magnets, Calculated from Multipole Expansion and From Polynomial Fitting

Component	Straight		Curved	
	FFT	Pol. Fit	FFT	Pol. Fit
B_1 (Dip.) [T m]	-3.46	-3.46	-3.46	-3.43
b_2[1] (Quad.) [10^{-4}]	-318.2	-287.4	236.1	275.6
b_3 (Sext.) [10^{-4}]	3.1	3.0	1.9	1.52
b_4 (Oct.) [10^{-4}]	-1.7	-2.0	2.5	5.15

[1] $b_n = \frac{B_n}{B_1}$

BEAM DYNAMICS SIMULATIONS

Particle tracking in the synchrotron lattice was performed using the Polymorphic Tracking Code (PTC) [12] interface in MAD-X, subject to the lattice parameters given in Table 2. Previous studies have been performed to optimise the overall design and to determine the optimal working point of the ring (Q_x = 1.68, Q_y = 1.13) [1]. The b_3 and b_4 multipoles were added to the start and end of each bending magnet, without a quadrupole (b_2) error, as the CT magnet is assumed to have the same b_2 as that of the CCT magnet. A small, realistic quadrupole error may be added for future simulations. The presence of these small gradient perturbations can introduce an amplitude dependent tune-shift, which can lead to particle losses and difficulties during extraction if the tune approaches lines of resonance. Single particles are tracked between (0 - 6$\sigma_{x,y}$) off the central beam trajectory at (x, y) = 0 to study the shift in tune for large deviation of particle positions as the beam circulates, and to indicate beam stability (the dynamic aperture, DA) over many turns. Initial parameters for particle tracking are given in Table 2 also. The β_x-functions of the unmodified lattice and of the lattice with multipole errors added to the start and end of each bending magnet are shown in Fig. 2 (top of the figure), along with the difference between the two, $\Delta\beta_x/\beta_{x_{\text{orig}}}$ (bottom of the figure), which represents the beta-beat.

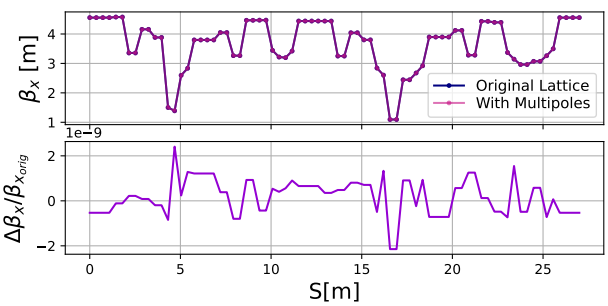

Figure 2: Simulated β_x of the unmodified lattice and of the lattice with multipole elements included in each bending magnet. The beta-beating is on the order of 10^{-9} due to the presence of sextupole and octupole errors.

ISBN: 978-3-95450-227-1 ISSN: 2673-5490 doi:10.18429/JACoW-IPAC2022-THPOMS028

To study the amplitude dependent tune shift introduced by these non-linear fields, we use action-angle variables $(J_{x,y}, \phi_{x,y})$, which are invariant during particle motion [13]. The relationship between (x, x') and (J_x, ϕ_x) is given by

$$\begin{pmatrix} x_N \\ x'_N \end{pmatrix} = \begin{pmatrix} \sqrt{2J_x}\cos\phi_x(s) \\ -\sqrt{2J_x}\sin\phi_x(s) \end{pmatrix} \quad (4)$$

Table 2: Parameters for the 27 m NIMMS Synchrotron ($\beta_{\text{rel}} = 0.73, \gamma_{\text{rel}} = 1.46$)

Parameter	Unit	Value
$E_{k_{\max}}$	MeV/u	430
$N_{\text{particles}}$	-	2×10^{10}
ε_{x_N}, ε_{y_N}	µm	(0.7, 1.0)
σ_x, σ_y	mm	(0.85, 1.78)
Q_x, Q_y	-	(1.68, 1.13)
ξ_x, ξ_y	-	(4.44, -7.24)

Results

Particles on momentum were tracked for 1024 turns. The tune was reconstructed from a precise FFT on each $J_{x,y}$ using the frequency analysis tool NAFFlib: a Python implementation of the NAFF (Numerical Analysis of Fundamental Frequencies) algorithm [14]. We use frequency map analysis (FMA) to scan the particles' phase space over many turns of tracking to determine the tune shift with amplitude, identifying regions of resonance [15, 16]. By splitting the turn data into two, we calculate a figure of merit D which represents the tune diffusion

$$D = \log_{10}\sqrt{\Delta Q_x^2 + \Delta Q_y^2} \quad (5)$$

A tune diffusion map is presented in Fig. 3, tracking particles at large amplitudes in (x, y) approaching the half-aperture (20 mm). The tune shift as a result of the multipoles is calculated to examine how much shift can be tolerated in the ring without significantly reducing the DA [13]. The DA was calculated from the stable region in Fig. 3, mostly preserved for tracking up to 6σ, with a slight reduction of 10% due to the presence of multipoles. The fractional tune as a function of J_x for this region is shown in Fig. 4, with similar results for J_y. The maximum tune shift $\Delta Q_x = 0.05$ at 6σ is obtained; the addition of multipoles to the bending magnets has introduced a small tune shift, which will be further examined after addition of fringe multipole fields. Up to the full aperture ($10\sigma_{x,y}$) the DA is reduced by 60%, suggesting that the multipole errors of the 30° CT magnet will need to be tuned accordingly.

The next step will be to parameterise the DA as a function of the strength of the errors to determine tolerable limits for the ring. For verification, replication of the study using other tracking codes (e.g. Zgoubi, RF-Track [17, 18]) is required. The lattice presented in this paper does not yet include resonant sextupoles for extraction; these will introduce additional non-linearities, thus affecting the amount of tune shift to be tolerated in the accelerator. These will be implemented in future studies.

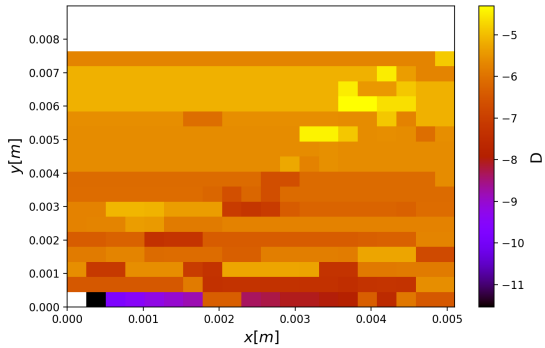

Figure 3: Initial conditions over an (x,y) grid, with D as a colour map representing the tune diffusion in the lattice for particles tracked between (0 - $6\sigma_{x,y}$). The color indicates the stability of the orbits; purple to dark orange (the lower part of the colourbar) show low diffusion orbits and yellow (the top of the colourbar) shows more chaotic orbits. White space indicates that a particle has been lost, apart from at (0,0), where $\Delta Q_{x,y}$ tends to zero due to maximum stability at this point.

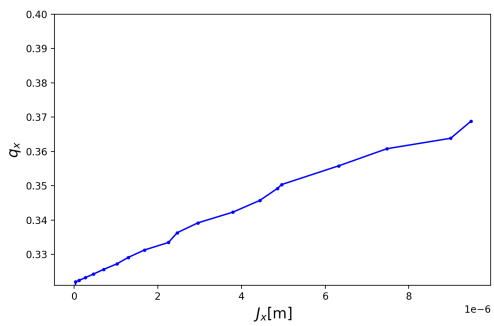

Figure 4: Fractional tune as a function of action, reconstructed from tracking particles between (0 - $6\sigma_{x,y}$) for the lattice with multipole errors.

CONCLUSION

An initial investigation using numerical analysis tools for the NIMMS superconducting synchrotron with curved magnet multipoles has been presented. The results from studying tune shift with action and the dynamic aperture of the ring indicate that the multipole errors must be parameterised in future simulations to fully gauge their effect. The study will be augmented to include resonant sextupoles and also fringe multipole terms in the magnets; results will be validated with other tracking codes before extending the study to a curved CCT magnet model for the NIMMS synchrotron.

ISBN: 978-3-95450-227-1 ISSN: 2673-5490 doi:10.18429/JACoW-IPAC2022-THPOMS028

REFERENCES

[1] E. Benedetto, N. A. Harbi, L. Brouwer, D. Tommasini, S. Prestemon, P. Riboni, *et al.*, "A Carbon-Ion Superconducting Gantry and a Synchrotron Based on Canted Cosine Theta Magnets," doi:10.48550/arXiv.2105.04205

[2] W. Wan, L. Brouwer, S. Caspi, S. O. Prestemon, A. Gerbershagen, J. M. Schippers, *et al.*, "Alternating-gradient canted cosine theta superconducting magnets for future compact proton gantries," *Physical Review Special Topics-accelerators and Beams*, vol. 18, p. 103501, 2015. doi:10.1103/PhysRevSTAB.18.103501

[3] J. B. Farr, J. B. Flanz, A. Gerbershagen, and M. F. Moyers, "New horizons in particle therapy systems," *Medical Physics*, vol. 45, pp. e953–e983, 2018. doi:10.1002/mp.13193

[4] "MAD-X,". URL: https://https://mad.web.cern.ch/mad/.

[5] U. Amaldi, N. Alharbi, E. Benedetto, P. Riboni, M. Vaziri, D. Aguglia, *et al.*, "SIGRUM - A Superconducting Ion Gantry with RIBONI'S Unconventional Mechanics," CERN, Geneva, Switzerland, CERN-ACC-NOTE-2021-0014 ; NIMMS-Note-002, 2021. http://cds.cern.ch/record/2766876/.

[6] M. Karppinen, V. Ferrentino, C. Kokkinos, and E. Ravaioli, "Design of a curved superconducting combined function bending magnet demonstrator for hadron therapy," *IEEE Transactions on Applied Superconductivity*, vol. 32, no. 6, pp. 1–5, 2022. doi:10.1109/TASC.2022.3155537

[7] D. I. Meyer and R. Flasck, "A new configuration for a dipole magnet for use in high energy physics applications," *Nuclear Instruments and Methods*, vol. 80, pp. 339–341, 1970. doi:10.1016/0029-554X(70)90784-6

[8] A. K. Jain, "Basic theory of magnets," in *CERN Accelerator School (CAS 97): Measurement and Alignment of Accelerator and Detector Magnets*, pp. 1–26, 1997.

[9] D. Veres, T. Vaszary, E. Benedetto, and D. Barna, "A New Algorithm for Optimizing the Field Quality of Curved CCT Magnets," *IEEE Transactions on Applied Superconductivity*, vol. 32, pp. 1–14, 3 2022. doi:10.1109/TASC.2022.3162389

[10] "Opera | SIMULIA by Dassault Systèmes,". https://www.3ds.com/products-services/simulia/products/opera/.

[11] A. Wolski, "Maxwell's equations for magnets," 2021. doi:10.48550/arXiv.1103.0713

[12] F. Schmidt, E. Forest, and E. McIntosh, "Introduction to the polymorphic tracking code: Fibre bundles, polymorphic Taylor types and "Exact tracking"," tech. rep., CERN, Geneva, Switzerland, Jul 2002.

[13] S. Y. Lee, "Accelerator physics, 4th edition," *Contemporary Physics*, vol. 60, no. 2, pp. 208–208, 2019. doi:10.1142/11111

[14] "GitHub - PyCOMPLETE/NAFFlib,". https://github.com/PyCOMPLETE/NAFFlib/.

[15] J. Laskar, "Frequency Map Analysis and Particle Accelerators", in *Proc. PAC'03*, Portland, OR, USA, May 2003, paper WOAB001, pp. 378 – 382.

[16] S. Antipov, S. Nagaitsev, and A. Valishev, "Single-particle dynamics in a nonlinear accelerator lattice: attaining a large tune spread with octupoles in IOTA," *Journal of Instrumentation*, vol. 12, p. P04008, 2017. doi:10.1088/1748-0221/12/04/p04008

[17] F. Méot, "Ray-tracing code Zgoubi," *Nuclear Instruments and Methods in Physics Research, Section A: Accelerators, Spectrometers, Detectors and Associated Equipment*, vol. 427, no. 1-2, pp. 353–356, 1999. doi:10.1016/S0168-9002(98)01508-3

[18] A. Latina, "Rf-track reference manual,", Zenodo. doi:10.5281/zenodo.3887085